

Superconducting quantum interference devices with submicron Nb/HfTi/Nb junctions for investigation of small magnetic particles

J. Nagel,¹ O.F. Kieler,² T. Weimann,² R. Wölbing,¹ J. Kohlmann,²
A.B. Zorin,² R. Kleiner,¹ D. Koelle,¹ and M. Kemmler^{1,*}

¹*Physikalisches Institut – Experimentalphysik II and Center for Collective Quantum Phenomena in LISA⁺,
Universität Tübingen, Auf der Morgenstelle 14, D-72076 Tübingen, Germany*

²*Fachbereich 2.4 "Quantenelektronik", Physikalisch-Technische Bundesanstalt, Bundesallee 100, 38116 Braunschweig, Germany*

(Dated: October 22, 2018)

We investigated, at temperature 4.2 K, electric transport, flux noise and resulting spin sensitivity of miniaturized Nb direct current superconducting quantum interference devices (SQUIDs) based on submicron Josephson junctions with HfTi barriers. The SQUIDs are either of the magnetometer-type or gradiometric in layout. In the white noise regime, for the best magnetometer we obtain a flux noise $S_{\Phi}^{1/2} = 250 \text{ n}\Phi_0/\text{Hz}^{1/2}$, corresponding to a spin sensitivity $S_{\mu}^{1/2} \geq 29 \mu_B/\text{Hz}^{1/2}$. For the gradiometer we find $S_{\Phi}^{1/2} = 300 \text{ n}\Phi_0/\text{Hz}^{1/2}$ and $S_{\mu}^{1/2} \geq 44 \mu_B/\text{Hz}^{1/2}$. The devices can still be optimized with respect to flux noise and coupling between a magnetic particle and the SQUID, leaving room for further improvement towards single spin resolution.

PACS numbers: 85.25.CP, 85.25.Dq, 74.78.Na, 74.25.F-

I. INTRODUCTION

Growing interest in the investigation of small spin systems like molecular magnets[1–3], single electrons [4] or cold atom clouds[5], demands for proper detection schemes. Compared to, e.g., magnetic resonance force microscopy [6] or magneto-optic spin detection [7, 8], superconducting quantum interference devices (SQUIDs) offer the advantage of direct measurement of changes of the magnetization in small spin systems [1, 9]. High spin sensitivity requires SQUIDs with low flux noise and strong magnetic coupling between particle(s) and SQUID loop. These needs can be met by nano-scaling the devices [10–12], e.g., by focused ion beam milling [13, 14], electron-beam lithography [15], atomic force microscopy anodization [16, 17], shadow evaporation [18] or by coupling small pickup loops to larger SQUIDs [19]. While nanopatterning of the SQUID loop yields no basic technical difficulties, the creation of overdamped Josephson junctions (JJs), as required for direct current (dc) SQUIDs, with submicron dimensions is more challenging. A widely used approach is to use constriction JJs. In some cases this yielded dc SQUIDs [14, 15] with root mean square (rms) flux noise $S_{\Phi}^{1/2}$ down to $0.2 \mu\Phi_0/\text{Hz}^{1/2}$ (Φ_0 is the magnetic flux quantum), which however are suitable only for operation in a limited range of temperature T . Even smaller $S_{\Phi}^{1/2} = 17 \text{ n}\Phi_0/\text{Hz}^{1/2}$ has been reported for larger SQUIDs based on superconductor-insulator-superconductor (SIS) tunnel JJs with external resistive shunts [20]. In this letter, we report on the realization of small and sensitive dc SQUIDs based on S-normalconductor (N)-S sandwich-type JJs, without resistive shunts, which simplifies SQUID miniaturization.

sec

II. SAMPLE FABRICATION AND LAYOUT

Our JJs are based on a Nb/HfTi/Nb trilayer process [21], which was developed for the fabrication of submicron SNS junctions [22]. All JJs are square shaped with lateral dimensions $200 \times 200 \text{ nm}^2$. The JJs with barrier thickness $d_{\text{HfTi}} = 24 \text{ nm}$ have a critical current density $j_c \approx 200 - 300 \text{ kA/cm}^2$ at $T = 4.2 \text{ K}$ and a resistance times junction area $\rho_n \approx 14 - 19 \text{ m}\Omega\mu\text{m}^2$, leading to a characteristic voltage $V_c = j_c\rho_n \approx 40 \mu\text{V}$. The three SQUIDs presented in this paper have different layouts. *G1* [see Fig. 1(a)] has a gradiometric design. The gradiometer line in the top Nb layer carries the bias current I (flowing through the junctions to the bottom Nb layer) and in addition allows for the (on-chip) application of magnetic flux Φ to the gradiometer (referred to one loop) via a current I_{mod} without the need of external coils. *M1* [see Fig. 1(b)] is of the magnetometer-type. *M2* [see inset of Fig. 1(b)], which is similar to *M1*, has a washer, allowing flux modulation with relatively small external magnetic fields ($B/\Phi = 0.5 \text{ mT}/\Phi_0$).

sec

III. EXPERIMENTS

All measurements were performed at $T = 4.2 \text{ K}$ in a high-frequency shielding chamber with the sample mounted inside a magnetic shield. All currents were applied by battery powered low-noise current sources. For the noise measurements we used a commercial Nb dc SQUID amplifier surrounded by a superconducting Nb shield [23]. The SQUID is connected in parallel to the input coil of the SQUID amplifier, with an input resis-

*Electronic address: matthias.kemmler@uni-tuebingen.de

tor R_{in} connected in series with the coil. A separate feedback (and modulation) coil of the SQUID amplifier allows for a flux locked loop operation of the SQUID amplifier with a sensitivity $S_{V,\text{amp}}^{1/2} \approx 40 \text{ pV/Hz}^{1/2}$ for $R_{\text{in}} = 3.3 \Omega$ at $T = 4.2 \text{ K}$. The typical bandwidth of the amplifier is of the order of few tens of kHz. To determine the rms flux noise of our SQUIDS we measured the voltage noise at the output of the amplifier. After subtracting the noise contribution from the amplifier, we obtain the spectral density of voltage noise $S_{V,\text{SQUID}}$ for the SQUID and calculate the corresponding rms flux noise $S_{\Phi}^{1/2} = S_{V,\text{SQUID}}^{1/2}/|\partial V/\partial \Phi|$. Here, V is the voltage across the SQUID and $\partial V/\partial \Phi$ is the transfer coefficient.

Figure 2(a) shows the current voltage characteristic (IVC) of $G1$ measured at $I_{\text{mod}} = 0$. The IVC is resistively shunted junction (RSJ)-like, with a critical current $I_c = 178 \mu\text{A}$ and resistance $R = 233 \text{ m}\Omega$, yielding $V_c = 41.5 \mu\text{V}$. The inset of Fig. 2(a) shows $I_c(I_{\text{mod}})$ together with a simulated curve based on the RSJ model (including thermal noise and inductance asymmetry), which yields $\beta_L \equiv 2I_0L/\Phi_0 = 0.18$. Here, I_0 is the average maximum critical current of the two JJs, and L is the inductance of the gradiometric SQUID, i.e. half the inductance of one loop of the gradiometer. With $2I_0 = 178 \mu\text{A}$ we obtain $L = 2.1 \text{ pH}$. From the measured period of $I_c(I_{\text{mod}})$ we obtain $\Phi/I_{\text{mod}} = 227 \text{ m}\Phi_0/\text{mA}$. The small but finite shift $\Delta I_{\text{mod}} = 95 \mu\text{A}$ of the maxima in $I_c(I_{\text{mod}})$ for opposite polarity can be solely attributed to an inductance asymmetry due to the asymmetric current bias, i.e. the asymmetry in the critical currents of the JJs is negligibly small. Figure 2(b) shows $V(I_{\text{mod}})$ for different values of I . For $I \approx 185 \mu\text{A}$ we obtain a maximum transfer coefficient $V_{\Phi} \approx 100 \mu\text{V}/\Phi_0$. The inset of Fig. 2(c) shows $V(I_{\text{mod}})$ and $S_{\Phi,w}^{1/2}(I_{\text{mod}})$ in the white noise regime (determined by averaging the spectra from $f = 2$ to 3 kHz) for $I = 185 \mu\text{A}$. This yields minima in $S_{\Phi,w}^{1/2}(I_{\text{mod}})$ at the optimum flux bias point (indicated by the dashed line), for which the main graph of Fig. 2(c) shows $S_{\Phi}^{1/2}$ vs frequency f . For low frequencies $f \leq 10 \text{ Hz}$ we find $S_{\Phi}(f) \propto 1/f^2$, which can

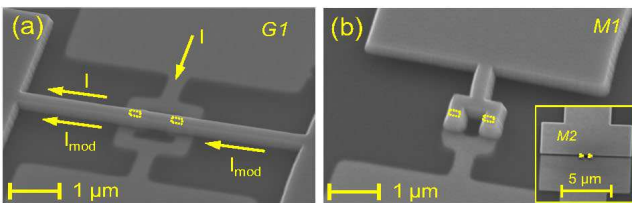


FIG. 1: (Color online) Scanning electron microscopy (SEM) images of the SQUIDS. The JJs with size $200 \times 200 \text{ nm}^2$ are indicated as dotted lines in the top Nb layer. (a) Gradiometer $G1$ with line width 250 nm and outer loop size $1.5 \times 1.5 \mu\text{m}^2$; arrows indicate scheme of current flow; (b) Magnetometer $M1$ with line width 250 nm and SQUID hole $500 \times 500 \text{ nm}^2$. Inset: washer-type magnetometer $M2$ with washer area $10 \times 10 \mu\text{m}^2$ and SQUID hole $500 \times 500 \text{ nm}^2$.

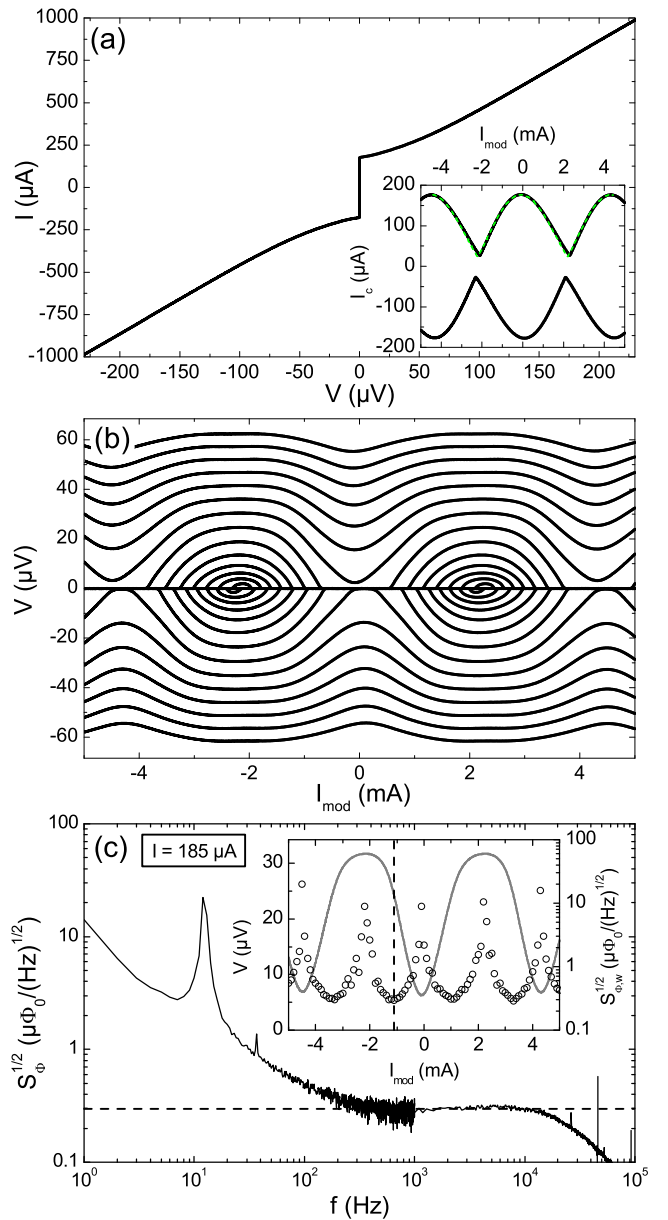


FIG. 2: (Color online) Transport and noise characteristics of $G1$ at $T = 4.2 \text{ K}$: (a) IVC at $I_{\text{mod}} = 0$; inset shows measured $I_c(I_{\text{mod}})$ (solid line) and simulated curve (dashed line). (b) $V(I_{\text{mod}})$ for $I = -297 \dots 300 \mu\text{A}$ (in $20.1 \mu\text{A}$ steps). (c) Spectral density of rms flux noise $S_{\Phi}^{1/2}(f)$ at optimal working point (c.f. dashed line in inset); dashed line indicates $300 \text{ n}\Phi_0/\text{Hz}^{1/2}$. Inset: $V(I_{\text{mod}})$ (solid line) and $S_{\Phi,w}^{1/2}(I_{\text{mod}})$ (open circles; averaged from $f = 2$ to 3 kHz).

be attributed to a single fluctuator (flux or I_c) producing random telegraph noise in the time trace $V(t)$. For higher frequencies $10 \text{ Hz} \leq f \leq 1 \text{ kHz}$ the frequency dependence is more $1/f$ like, which might be caused by an admixture of noise from a few additional fluctuators with higher characteristic frequencies. The peak in $S_{\Phi}(f)$ near $f = 12 \text{ Hz}$ presumably results from mechanical vibrations. The spectrum in the white noise limit above

1 kHz yields $S_{\Phi,w}^{1/2} \approx 300 \text{ n}\Phi_0/\text{Hz}^{1/2}$, with a cutoff at $f \approx 2 \times 10^4 \text{ Hz}$ due to the SQUID amplifier electronics. The magnetometer-type devices *M1* and *M2* had similar characteristics, with $S_{\Phi,w}^{1/2} \approx 250 \text{ n}\Phi_0/\text{Hz}^{1/2}$ and $\approx 270 \text{ n}\Phi_0/\text{Hz}^{1/2}$, respectively.

sec

A. estimated Spin sensitivity

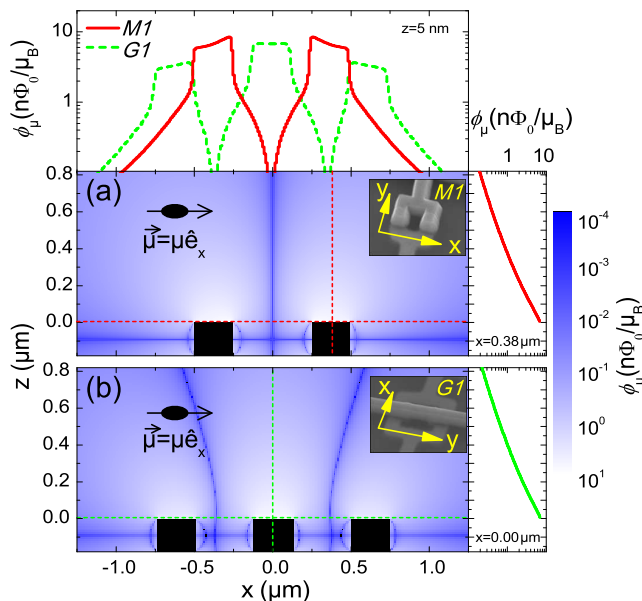


FIG. 3: (Color online) Calculated coupling factor ϕ_μ vs particle position. Main graphs show contour plots $\phi_\mu(x, z)$ for (a) magnetometer *M1* and (b) gradiometer *G1*; Nb structures are indicated by black rectangles. Insets show SEM images of the SQUIDs. Dashed lines indicate position of linescans $\phi_\mu(x)$ [shown above (a)] and $\phi_\mu(z)$ [shown to the right of (a) and (b)].

Finally, we turn to the spin sensitivity $S_\mu^{1/2} = S_\Phi^{1/2}/\phi_\mu$ of our devices which, besides the flux noise, depends on the coupling factor ϕ_μ , i.e. the amount of flux coupled into the SQUID by a magnetic particle, divided by the modulus $|\vec{\mu}|$ of its magnetic moment. Taking into account the SQUID geometry, Fig. 3 shows the calculated coupling factor of *M1* and *G1* vs. the position \vec{r} of a point-like magnetic particle with its magnetic moment $\vec{\mu}$ pointing in-plane of the SQUID loop. A detailed description of the calculation procedure for non-gradiometric SQUIDs can be found in Ref. [12]. For the gradiometric SQUID *G1*

one has to consider the magnetic field distribution $\vec{B}(\vec{r})$ created by two circular currents $I_{1,2} = \pm I_B$ in each loop. In this case the coupling factor ϕ_μ is given by $\vec{B}(\vec{r})/2I_B$. For an in-plane magnetization of the particle, layout *M1* provides the highest coupling factor if the particle is placed directly on top of the SQUID loop. For *G1* the optimum coupling can be achieved if the particle is placed on the center conductor line. At this position the particle couples flux of opposite sign into both loops of the gradiometric SQUID, which leads to an approximately twice as large coupling factor as compared to placing the particle on the outer conductors. For a particle with 10 nm diameter, placed directly on top of the SQUID surface, which yields $\phi_\mu = 8.5 \text{ n}\Phi_0/\mu_B$ (μ_B is the Bohr magneton) for *M1* and $6.8 \text{ n}\Phi_0/\mu_B$ for *G1* at the center conductor. With $S_\Phi^{1/2} \approx 250 \text{ n}\Phi_0/\text{Hz}^{1/2}$ we calculate the spin sensitivity of *M1* to $S_\mu^{1/2} = 29 \mu_B/\text{Hz}^{1/2}$. For the gradiometric SQUID we calculate $S_\mu^{1/2} = 44 \mu_B/\text{Hz}^{1/2}$.

sec

IV. CONCLUSIONS

In conclusion, we have shown that miniaturized dc SQUIDs based on sandwich-type overdamped SNS Josephson junctions have a compact design and can be operated with very promising values of flux noise and spin sensitivity. Although our devices are not optimized yet, flux noise values down to $250 \text{ n}\Phi_0/\text{Hz}^{1/2}$ have been achieved, leading to an estimated spin sensitivity as low as $29 \mu_B/\text{Hz}^{1/2}$. Further improvements are feasible; e.g., placing the two SQUID arms on top of each other, as in Ref.[20], allows for reduction of the SQUID inductance and hence of the flux noise. Furthermore, the coupling can be improved by patterning an additional constriction within the SQUID loop.

sec

Acknowledgment

This work was supported by the Nachwuchswissenschaftlerprogramm of the Universität Tübingen, by the Deutsche Forschungsgemeinschaft (DFG) via the SFB TRR21 and by the European Research Council via SOCATHES. J. Nagel and M. Kemmler gratefully acknowledge support by the Carl-Zeiss Stiftung.

[1] W. Wernsdorfer, Adv. Chem. Phys. **118**, 99 (2001).
 [2] D. Gatteschi and R. Sessoli, Angew. Chem., Int. Ed. **42**, 268 (2003).

[3] L. Bogani and W. Wernsdorfer, Nature Materials **7**, 179 (2008).
 [4] P. Bushev, D. Bothner, J. Nagel, M. Kemmler, K. B.

- Konovalenko, A. Loerincz, K. Ilin, M. Siegel, D. Koelle, R. Kleiner, and F. Schmidt-Kaler, *Eur. Phys. J. D*(2011).
- [5] J. Fortágh and C. Zimmermann, *Science* **307**, 860 (2005).
- [6] D. Rugar, R. Budakian, H. J. Mamin, and B. W. Chui, *Nature* **430**, 329 (2004).
- [7] J. R. Maze, P. L. Stanwix, J. S. Hodges, S. Hong, J. M. Taylor, P. Cappellaro, L. Jiang, M. V. Gurudev Dutt, E. Togan, A. S. Zibrov, A. Yacoby, R. L. Walsworth, and M. D. Lukin, *Nature* **455**, 644 (2008).
- [8] G. Balasubramanian, I. Y. Chan, R. Kolesov, M. Al-Hmoud, J. Tisler, C. Shin, C. Kim, A. Wojcik, P. R. Hemmer, A. Krueger, T. Hanke, A. Leitenstorfer, R. Bratschitsch, F. Jelezko, and J. Wrachtrup, *Nature* **455**, 648 (2008).
- [9] J. Gallop, *Supercond. Sci. Technol.* **16**, 1575 (2003).
- [10] C. P. Foley and H. Hilgenkamp, *Supercond. Sci. Technol.* **22**, 064001 (2009).
- [11] V. Bouchiat, *Supercond. Sci. Technol.* **22**, 064002 (2009).
- [12] J. Nagel, K. B. Konovalenko, M. Kemmler, M. Turad, R. Werner, E. Kleisz, S. Menzel, R. Klingeler, B. Büchner, R. Kleiner, and D. Koelle, *Supercond. Sci. Technol.* **24**, 015015 (2011), 1009.2657.
- [13] A. G. P. Troeman, H. Derking, B. Borger, J. Pleikies, D. Veldhuis, and H. Hilgenkamp, *Nano Lett.* **7**, 2152 (2007).
- [14] L. Hao, J. C. Macfarlane, J. C. Gallop, D. Cox, J. Beyer, D. Drung, and T. Schurig, *Appl. Phys. Lett.* **92**, 192507 (2008).
- [15] R. F. Voss, R. B. Laibowitz, and A. N. Broers, *Appl. Phys. Lett.* **37**, 656 (1980).
- [16] V. Bouchiat, M. Faucher, C. Thirion, W. Wernsdorfer, T. Fournier, and B. Pannetier, *Appl. Phys. Lett.* **79**, 123 (2001).
- [17] M. Faucher, P.-O. Jubert, O. Fruchart, W. Wernsdorfer, and V. Bouchiat, *Supercond. Sci. Technol.* **22**, 064010 (2009).
- [18] A. Finkler, Y. Segev, Y. Myasoedov, M. L. Rappaport, L. Neeman, D. Vasyukov, E. Zeldov, M. E. Huber, J. Martin, and A. Yacoby, *Nano Lett.* **10**, 1046 (2010).
- [19] N. C. Koshnick, M. E. Huber, J. A. Bert, C. W. Hicks, J. Large, H. Edwards, and K. A. Moler, *Appl. Phys. Lett.* **93**, 243101 (2008).
- [20] D. J. Van Harlingen, R. H. Koch, and J. Clarke, *Appl. Phys. Lett.* **41**, 197 (1982).
- [21] D. Hagedorn, R. Dolata, F.-I. Buchholz, and J. Niemeyer, *Physica C* **372–376**, 7 (2002).
- [22] D. Hagedorn, O. Kieler, R. Dolata, R. Behr, F. Müller, J. Kohlmann, and J. Niemeyer, *Supercond. Sci. Technol.* **19**, 294 (2006).
- [23] SQ100 LTS dc SQUID, PC-100 Single-Channel dc SQUID Electronics System, STAR Cryoelectronics, USA.